CTAB mediated Calcination-Free Hydrothermal Reaction Mechanism and Electrochemical Study of Zn_2SnO_4 (ZSnO) Nanoflakes

Sana Hanif
Islamia University of Bahawalpur, Baghdad-ul-Jadeed Campus

Syed Mustansar Abbas
National Centre for Physics, Quaid-i-Azam University Campus

Khalil-ur-Rehman
Kohat University of Science and Technology (KUST)

https://doi.org/10.5109/7395626

出版情報：Proceedings of International Exchange and Innovation Conference on Engineering & Sciences (IEICES). 11, pp.947-954, 2025-10-30. International Exchange and Innovation Conference on Engineering & Sciences
バージョン：

CTAB mediated Calcination-Free Hydrothermal Reaction Mechanism and Electrochemical Study of Zn_2SnO_4 (ZSnO) Nanoflakes

Sana Hanif[1], Syed Mustansar Abbas[2], Khalil-ur-Rehman[3]

[1] Islamia University of Bahawalpur, Baghdad-ul-Jadeed Campus, 63100, Bahawalpur, Pakistan
[2] National Centre for Physics, Quaid-i-Azam University Campus, Islamabad 44000, Pakistan
[3] Kohat University of Science and Technology (KUST), Bannu Road, Kohat 26000, Khyber Pakhtunkhwa, Pakistan
Corresponding author: sanahanif150@gmail.com

Abstract: *The enormous surface area and tunable shape of metal oxides have made them attractive candidates for energy storage applications. In this work, Zn_2SnO_4 (ZSnO) were prepared to find the electrochemical properties of the ultimate pseudocapacitive electrode using a CTAB-mediated one-step hydrothermal process that did not include calcination. To study the hydrothermal process, chemical pathways were followed step-by-step. Electrochemical measurement, XRD, SEM, FTIR, and DRS were used to analyze the structural, morphological, and electrochemical properties. The usual crystallite size of (ZSnO) in a spinel structure is roughly 13 nm, according to XRD measurements. Although electrochemical behavior was unaffected, FTIR research also verified that CTAB was removed during synthesis. During the electrochemical test, ZSnO displayed 27.49 Fg^{-1} specific capacitance, 0.0764 Wg^{-1} power density, and 0.9545 Whg^{-1} energy density at a current density of 0.35A/g. These findings provide credence to the use of Zn2SnO4 (ZSnO) as a pseudo capacitor electrode and demonstrate the efficacy of morphological control by surfactant-assisted synthesis.*

Keywords: CTAB as surfactant, Hydrothermal Synthesis, Nanoflakes, Electrochemical Performance

1. INTRODUCTION

In response to the global energy crisis and the growing need for portable, reliable electronics, scientists set out to develop a sustainable energy storage system that could maximize power output while keeping the environment safe [1-2]. We need renewable, clean, alternative, and affordable energy sources to solve the energy and environmental crises [3-4]. Supercapacitors and lithium-ion batteries are electrical energy storage devices that are necessary to maximize the use of renewable energy sources such as wind and solar [5-7], which are fundamentally unpredictable.

An essential part of many energy storage systems, supercapacitors (SCS) outperform lithium-ion batteries in terms of power density, charging speed, and lifespan [8]. As a result, several studies are being conducted to discover new methods of enhancing the energy density values of supercapacitors, with a focus on exploring innovative electrode materials [9-10]. According to some sources, this is one way to get a high specific capacitance, leading to a high energy density [11-14]. Due to their superior power and energy density compared to conventional batteries and dielectric capacitors, electrochemical supercapacitors have piqued the attention of many researchers [15].

The selection of electroactive materials is influenced by the supercapacitor application, which requires a high-power density, and the choice of electrode material significantly impacts the supercapacitor's performance [16-20]. The abundance, low cost, lack of toxicity, and ease of modifying the morphological and structural features of nanoparticles synthesized by metal oxides to suit their intended uses have piqued the interest of researchers throughout the globe [21]. Ternary metal oxides, including Zn2SnO4 and Zn2TiO3, have lately arisen as attractive substitutes for the more traditional binary metal oxides, commonly recognized as excellent semiconductor materials for these uses. Because of its appealing optoelectronic characteristics, low absorption of visible light, high electrical conductivity, and high electron mobility, the A_2BO_4 inverse spinel structure of zinc stannate (Zn_2SnO_4) opens up a world of possibilities in optics, photocatalysis, solar cells, photodegradation, gas sensing, and more [22-29]. There have been recent successes in developing hydrothermal synthesis techniques to create Zn2SnO4. This approach is auspicious for practical manufacturing since it is inexpensive and safe for the environment [30-34]. Given the general knowledge that ZnO evaporates quickly when heated, methods that operate with high temperatures cannot produce the Zn_2SnO_4 phase [35,36].

This work synthesized CTAB assisted calcination free Zn_2SnO_4 (ZSnO) nanoparticles by a straightforward hydrothermal technique. The synthesized products have been characterized, and the electrochemical characteristics of the samples, have been examined and documented. To the best of our knowledge, it would be

the first report that describes effect of surfactant (CTAB) on morphology and its electrochemical behaviour without heating effect.

2. MATERIALS AND METHODS

High-purity $ZnCl_2$ and $SnCl_2.2H_2O$ are required in a 2:1 ratio to make Zn_2SnO_4 (ZSnO). All reagents were analytical grade without purification. The first stage involves magnetically stirring ethanol with a 2M zinc chloride ($ZnCl_2$) solution, 10 mM (NaOH) and 20ml CTAB at room temperature for 20 minutes.
After that, 1 M $SnCl_2.2H_2O$ is dissolved in ethanol and incorporated gradually into the mixture while being stirred magnetically to produce a whitish slurry. After 30 minutes of stirring, the slurry was loaded to 80% capacity into a Teflon-coated stainless-steel autoclave. The autoclave was let to cool to ambient temperature after being heated to 200 °C for 24 hours. The precipitation was then removed and washed with distilled water and ethanol. Then, particles were washed and then dried at 80 °C for 20 hours.
The following reaction equation describes the production of ZSnO by using CTAB as surfactant that doesn't take part in chemical reactions, enhance the morphology, during this hydrothermal treatment:

$$2ZnCl_2 + SnCl_2 \cdot 2H_2O + 6NaOH \rightarrow Zn_2SnO_4 \text{ (solid)} + 6NaCl + 5H_2O \quad \text{----------(1)}$$

3. ELECTRODE PREPARATION AND ELECTROCHEMICAL MEASUREMENTS

N-methyl-2-pyrrolidone was used to combine the powders with conductive reagents, active material, and PVDF, a binder. In certain situations, a lot of carbon reagent was employed to investigate the powders' electrochemical activity. It was rinsed with HCl and acetone and oven-dried to activate Ni Foam. The slurry was agitated with a magnetic plate at room temperature for 3–5 hours. A nickel foam (1 cm-2) current collector, for example, which serves as the electrode, is spread out uniformly across a conductive substrate before the slurry is added. The solvent is evaporated, and the active ingredient is solidified after 12 hours of drying the coated substrate at high temperatures. This substance's mass was estimated using a microbalance. Dry electrodes were built for electrochemical examination in the testing cell.

In a standard three-electrode setup, electrochemical measurements were carried out utilizing GAMRY Station. These included a reference electrode made of Ag/AgCl, a high-purity platinum-wire counter electrode, and a sample-working electrode. The three-electrode cell's aqueous electrolyte and nickel foam current collector were both treated with the nanocomposite. Aqueous electrolytes are cheaper than organic or ionic solutions. The three-electrode cell arrangement has an active electrode material mass of about 20 mg. Impedance measurements was carried out with frequency range of 100 kHz to 0.1 Hz at room temperature, we calculated the specific capacitance, energy density, and power density using the formulae below:

$$Cp = I^* \Delta t / m^* \Delta V \quad \text{----------(2)}$$

The variables m, I, t, and V represent the mass of the active material, the potential window, the discharge time, and the current, respectively.

$$Eg = (1/2(Cp\ (\Delta V)^2)\ /3600 \quad \text{----------(3)}$$
$$Pg=(E\ *3600)/\Delta t \quad \text{----------(4)}$$

Pg stands for power density in W/g, Δt for discharge time, ΔV for potential window, and Eg for energy density in Wh/g.

4. MATERIAL CHARACTERIZATION

The crystal phases were discovered with a scan rate of 1°/min using X-ray diffraction analysis, namely the XRD Rigaku with Cu-Kα radiation and a λ value of 1.5418 Å, throughout the range of (2θ = 20-80°). A scanning electron microscope (FE-SEM-JEOL-2010) with an accelerating voltage of 100 kV was used to characterize the morphological material. To assess chemical bonding in the 4000-400 cm^{-1} range, the Jasco FT/IR 6600 apparatus is used. A Perkin Elmer Lambda Diffuse Reflectance spectrometer produced the absorption spectra of Zn_2SnO_4 nanoparticles in the 200-800 nm wavelength range.

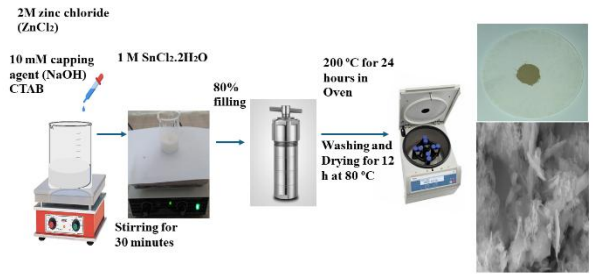

Fig 01: Schematic illustration of hydrothermally synthesized Zn_2SnO_4 (ZSnO)

5. RESULTS AND DISCUSSIONS

Fig. 02 shows XRD patterns that analyze the products' crystallographic structure and phase purity. At 200 °C, Zn_2SnO_4 (ZSnO) is the predominant product owing to its decreased solubility in the reaction Eq. (9). Upon thermal breakdown of $Zn(OH)_4^{2-}$, the precipitate of ZnO and Zn_2SnO_4 (spinel ZSnO) is produced (Eqs. (10)). Not only does the sample include Zn_2SnO_4 (ZSnO) nanoparticles with a lattice constant of 8.657 Å and a space group of Fd-3m, but it also contains wurtzite ZnO (ICSD 36–1451).
The peaks have an inverted spinel structure with half of the Zn^{2+} atoms coordinated tetrahedrally, and all of the Sn^{4+} atoms coordinated octahedral [41]. Nanoparticles are approaching the anticipated stoichiometric ratio, as seen by the XRD pattern, which indicates that the reaction is complete [42]. The XRD line broadening of firm peaks was used to measure the particles' crystallite size using Scherer's equation:

$D=K*\lambda/\beta\cos\theta$ ----------(5)

Where λ is wavelength, β is full width half maxima, and K (0.94) is a constant.
The average particle size is about 13 nm, which aligns with previous research [43]. The ZSnO nanowires have excellent crystallinity due to prominent, crisp X-ray diffraction peaks. When sodium hydroxide is present during the first stage of a hydrothermal process, complex forms such as $ZnSn(OH)_6$ and $Zn(OH)_4^{2-}$ are produced. Hydrothermal treatment, which involves very high temperatures and pressures, further breaks down these complex structures into Zn_2SnO_4 nnanoparticles [34,44,45]. The process of reaction is as follows.

$Zn^{+2} + Sn^{+4} + 6OH^- \rightarrow ZnSn(OH)_6$ ----------(6)

Under severe alkaline conditions, a mixed metal hydroxide complex develops.

$ZnSn(OH)_6 + 4OH^- \rightarrow Zn(OH)^{2-}_4 + ZnSn(OH)^{2-}_6$ ---(7)

$ZnSn(OH)^{2-}_6$ decomposes into a metastable intermediate phase, $ZnSnO_3$.

$ZnSn(OH)^{2-}_6 \rightarrow ZnSnO_3 + 3H_2O$ ----------(8)

The interaction of $ZnSnO_3$ with extra Zn^{2+} finalizes the creation of Zn_2SnO_4 (spinel-type oxide).

$ZnSnO_3 + Zn^{+2} + 2OH^- \rightarrow Zn_2SnO_4 + H_2O$ ----------(9)

$Zn(OH)^{2-}_4 \rightarrow ZnO + H_2O + 2OH$ ----------(10)

Side reaction producing ZnO dependent on local pH and Zn^{2+} surplus.

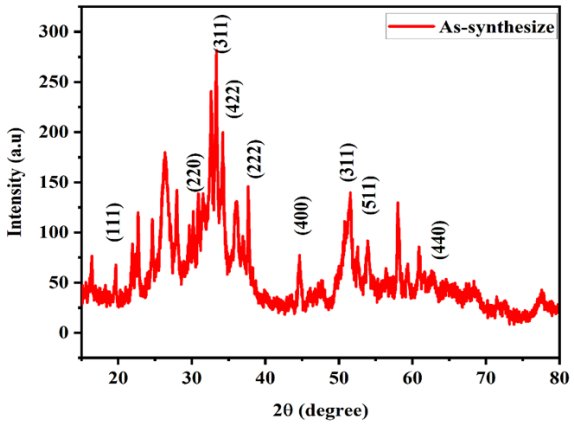

Fig 02: XRD results of as-synthesized ZSnO Pseudocapacitive material

To assess the surface treatment and chemical composition of room-temperature ZSnO nanoparticles, FTIR spectroscopy was used in the 400-4000 cm^{-1} band. The **figure 03** displays the FTIR spectra of CTAB mediated as-synthesized ZSnO. An absorption peak around 503.76 cm^{-1} is due to Sn-O-Zn bond in the ZSnO material. An absorption peak at 1638.50 cm^{-1} represents H-O-H bonding while 3497.60 cm^{-1} is supposedly caused by a O-H stretching bond, as stated in the reference [46]. The Zn bonding causes the peak at 2300 cm^{-1}, whereas the peak at 1167.76 cm-1 is associated with the Sn-O stretching vibration in ZSnO [47.10]. It is also seen that there are no major peaks related to CTAB appeared in ZSnO (C-N, C-H stretching), however, peak around 2943 might be associated to residual CTAB due to surface adsorbed organic or hydroxyl groups. Similar peak also observed in ZSnO sample. Thus, presence of CTAB in final product is negligible as sample was washed and dried and it doesn't affect electrochemical behavior.

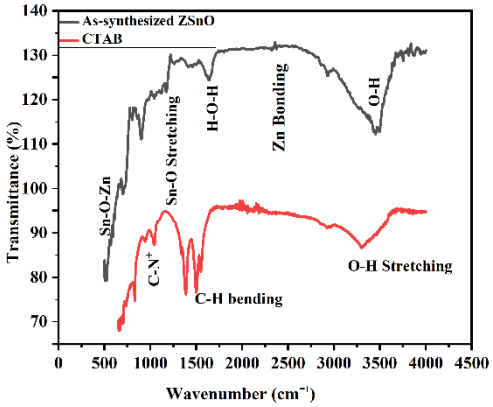

Fig 03. FTIR images of as-synthesized ZSnO Pseudocapacitive material

Fig. 04 shows the produced ZSnO nanoparticles' reflectance spectra. The peak absorption at 310 nm is indicative of Zn_2SnO_4 (ZSnO) [11]. A reflectance edge is readily seen in Zn_2SnO_4, suggesting that this is not attributable to impurity-level transitions but to intrinsic semiconductor transitions [46-49].
The Tauc graphs and the Kubelka-Munk (K-M) formula determine the band gap. The fact that Zn_2SnO_4 is a direct semiconductor allows one to calculate Eg by graphing the optical band gap $(\alpha h\upsilon)^2$ against $h\upsilon$. The bandgap Eg value of 3.30 eV is obtained from the Tauc plot, which is shown in **Figure 04**, for the synthesized ZSnO nanoparticles. Younge et al. [48] found a similar outcome when they intersected the extrapolated linear segment with the x-axis. On the other hand, 3.1 eV was reported as the fundamental bandgap of Zn_2SnO_4 by Shi and Dai et al. [49-50]. Despite ongoing debates concerning Zn_2SnO_4's optical absorption characteristic, our single-crystalline Zn_2SnO_4's calculated bandgap value agrees with other publications [51-53].

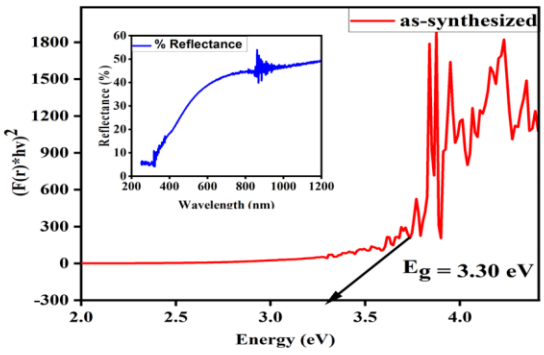

Fig 04: Diffuse Reflectance spectroscopy and Bandgap illustration of as-synthesized ZSnO Pseudocapacitive material

The SEM image of ZSnO nanoparticles is shown in **Figure 05**. Nanostructures in CTAB mediated as-synthesized sample display the flakes like hierarchical

morphologies as seen in **Fig 05**. As FTIR also depicts its removal after washing, thus, CTAB act as surfactant directed agent in our synthesis. CTAB micelles leads to increased surface area and improved electrolyte diffusion pathways which is positive act for electrochemical performance. Rapid nucleation and slow crystal development produce this shape, consistent with XRD findings and often yield structures with poor crystallinity [54]. The nanoflakes shows an image of several dispersed but organized flowers representing a cluster [55]. Multiple factors, including precursor solution sodium hydroxide concentration, reaction time, surfactant and temperature, influence the final ZSnO nanoparticle size and shape [56].

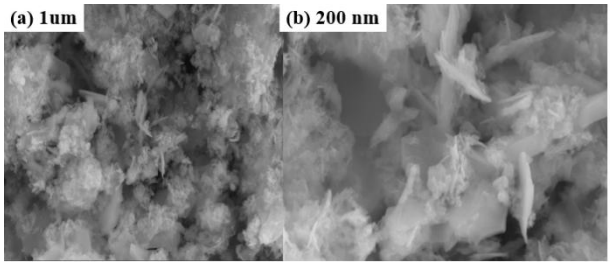

Fig 05: SEM images of as-synthesized ZSnO Pseudocapacitive material

Cyclic voltammetry studies were performed using scan speeds of 5, 10, 30, 50, 70, and 100 mV/s to explore the electrochemical kinetics of ZSnO. The **figure 06** depicts pseudo-capacitive behavior characterized by faradaic redox processes predominating in the cationic and anionic portions. When Zn ions are present in the interplane of tin oxide, they enhance the cyclic stability of the active materials by controlling the diffusion of Sn ions. When the scan rate is increased inside a constant potential frame, it is shown that the sample's specific capacitance decreases as well [10,11]

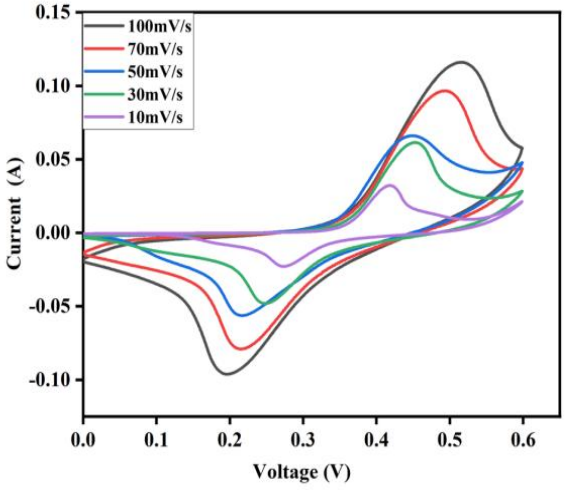

Fig 06: Cyclic Voltammetry results of PVDf bound calcination free as-synthesized ZSnO Pseudocapacitive material at different scan rates

A reduced pseudo capacitance contribution was seen from the device at faster sweep rates since the ions only interacted with the outer electrode and the bulk material within the pores, owing to minimal or no interactions [18]. The anodic curve shows electrode oxidation during the positive linear voltage sweep. The rapid and efficient reversible electrode response caused the CV capacitive curve to invert during discharge and the cathodic current to reach its maximum value. Improved electrochemical activity is partly due to the active material's rapid diffusion of electrolytic ions. When Zn_2SnO_4 reacts with OH^- and H_2O during cycling, it may carry out surface redox processes. This mechanism leads to pseudocapacitive charge storage, as the electron transfer (e^-) shows. Consider the following equation:

$$Sn^{+2} \leftrightarrow Sn^{+4}+2e^- \text{ ----------(11)}$$

$$Zn_2SnO_4 + OH^- + H2O \rightarrow SnOOH +2ZnOOH+ e^- \text{----(12)}$$

There is a discernible shift in the redox potential as well, more especially, there is a little shift in the charge transfer resistance as the scan rate increases due to faster electron transport kinetics. CV curves maintain its redox shape even at higher scan rates due to materials' strong redox capacitive properties. Supporting the idea that ZSnO might be a high-power supercapacitor, the fact that the redox-CV curves stay the same even when scanning at greater speeds is encouraging [53].

The samples' capacitive properties were investigated by the GCD tests, as seen in **Figure 07**, by applying voltage 0-0.6V and multiple current densities 0.05, 0.15, 0.35, and 0.50 A g^{-1} with applied currents (1, 3, 7, and 10 mA).The Cp (specific capacitance), Pg(power density) and E_g(energy density) are calculated from the above formula (**Eq. 2,3 and 4)**, which is about 19.54F/g, 0.1141W/kg, 25.57Wh/kg. During charging and discharging, it is evident that all GCD curves have nonlinear voltage platforms, which are characterized by noticeable voltage plateaus. Previous studies [54] have shown that this behavior may be explained by the reversible redox transition between Sn^{2+} and Sn^{4+} one (Eq.11). To store energy, Sn^{2+} is oxidized to Sn^{4+} when it is charged. Upon discharge, Sn^{+2} is converted to Sn^{4+}, releasing the stored energy.

This change enables electron transport at the point where the electrode and electrolyte come into contact. As seen in **Fig.07,** the charge/discharge time rose in inverse proportion to the potential window.

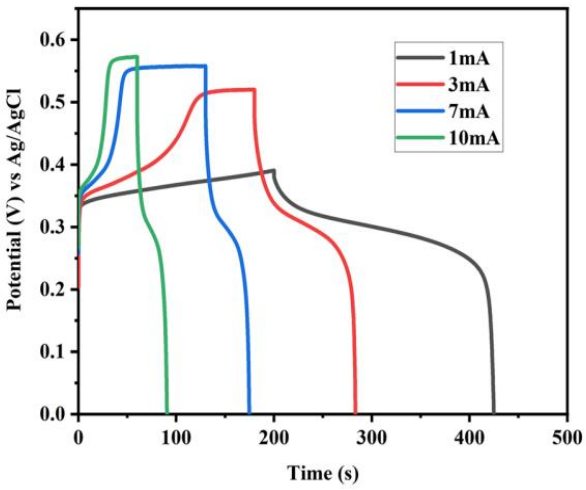

Fig 07: Galvano charge-discharge of PVDf bound calcination free as-synthesized ZSnO Pseudocapacitive material at different current rates

Because some active spots on the material's surface prevent charge storage, ZSnO-based electrodes exhibit the best capacitor capabilities at high current densities, allowing the charge and discharge to grow rapidly. The even distribution of particles on the surface of the electrode allows for the intercalation of charge carriers between the electrolyte and the electrode, which might explain why these electrodes have a charging and discharging cycle life that is rather lengthy [55]. Reduced IR drop during discharge is a consequence of the electrode's low internal resistance, which is a consequence of the particles' regular organization; this leads to an improvement in the transport of ions from electrolyte to the surface of electrode [56].

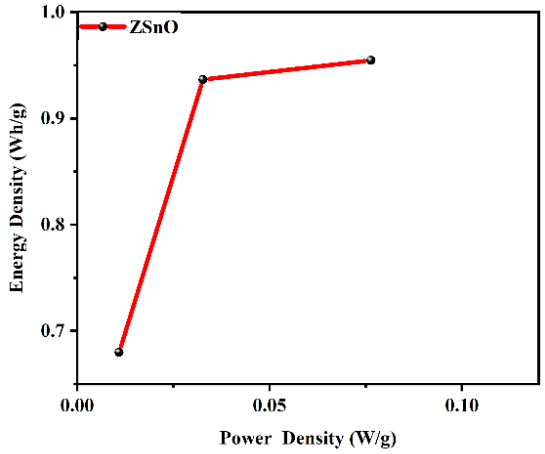

Fig 08: Regression Plot between E_g and Pg of PVDf bound calcination free ZSnO electrode observed at current Density of 0.05,0.15 and 0.35A/g.

As seen in **Figure 08**, lower energy densities are correlated with greater power densities. With a current density of 0.35A/g and an energy storage capacity of 0.9545 Wh/g at 0.0765 W/g, the as-synthesized electrode has the best charge-discharge capabilities and the largest energy storage capacity. This performance is probably made possible by the redox activity of Sn^{2+}/Sn^{+4} species, which suggests a method for pseudocapacitive charge storage. The material's ability to steadily decrease energy density with increasing power density demonstrates its ability to give an adequate amount of energy even under more demanding current loads, which is ideal for hybrid supercapacitors that need rapid charge delivery and limited energy storage.

To further investigate the kinetics of ZSnO recombination and interface charge transfer, EIS was conducted as shown in **Figure 09**. There is a Nyquist plot with depressed semicircle in the high-frequency region of the Nyquist plot. Afterwards, in the low frequency region, a 45° inclined Warburg line indicates a combined charge transfer and diffusion process. An analogous circuit to R(Q(RW)) was used to fit the data using a Gamry Echem analyzer (refer to the inset of **Figure 09**). An analogous circuit that incorporates CPE (Constant phase element) and Warburg element to regulate ion diffusion, Rct, and Rs used to match the EIS data. The synthesized sample showed an Rs value of 0.89 ohm and an Rct value of roughly 3.21 ohm, which conforms with the literature [11,18,56]. The low semicircle diameter in the Nyquist plot indicates that the charge transport was more efficient due to the excellent crystallinity [57].
A high electrochemically active surface area allowed for the very efficient transit of electrons and electrolytic ions, as seen by the low electrolyte solution resistance (Rs).

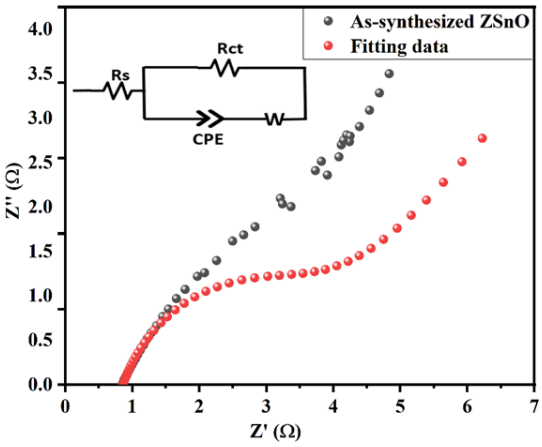

Fig 09: Nyquist plot of PVDf bound calcination free as synthesized and fitted data of ZSnO Pseudocapacitive material, the inset figure shows an equivalent circuit

Supercapacitors' high specific power is due to their low Faraday resistance [58]. A reduced Rct improves reactions, and the electrochemical performance of ZSnO is confirmed by both electrochemical responses. The CV curves in Figure 6 agree with the EIS findings.

6. CONCLUSION

In this work, Zn2SnO4 (ZSnO) nanoflakes were fabricated by CTAB-mediated hydrothermal synthesis without calcination. CTAB played vital role in developing hierarchical morphology as confirmed by SEM-analysis. FTIR results shows that CTAB was removed after synthesis that ensures a good and effective surface area for its electrochemical performance as pseudocapacitive electrode. The crystallite size was calculated to be 13 nm, by XRD analysis. CTAB mediated and calcination free ZSnO electrode has pseudocapacitive character in their electrochemical performance, with a redox peak occurring within a broad potential window. Thus, research has shown that ZSnO nanoparticles have good electrochemical capabilities and yet CTAB just used to control the morphology of as-synthesized sample.

7. ACKNOWLEDGMENT

The author expresses gratitude to the National Centre for Physics, Islamabad, for providing research resources throughout the master's program under the guidance of Dr. Syed Mustansar Abbas and Dr. Gul Naz.

8. REFERENCES

1. Li, C., Balamurugan, J., Kim, N. H., & Lee, J. H. (2018). Hierarchical Zn–Co–S nanowires are advanced electrodes for all asymmetric

supercapacitors. *Advanced Energy Materials*, *8*(8), 1702014.
2. Erdem, E. "Why P2X must be the part of the energy solution?." *Environmental progress & sustainable energy* 40.3 (2021): e13545.
3. Li, Yang, et al. "Fe2O3 nanoneedles on ultrafine nickel nanotube arrays as efficient anode for high-performance asymmetric supercapacitors." *Advanced Functional Materials* 27.14 (2017): 1606728.
4. Wu, Runze, et al. "MgCo 2 O 4-based electrode materials for electrochemical energy storage and conversion: a comprehensive review." *Sustainable Energy & Fuels* 5.19 (2021): 4807-4829.
5. Samuel, Edmund, et al. "Supersonically sprayed Zn2SnO4/SnO2/CNT nanocomposites for high-performance supercapacitor electrodes." *ACS Sustainable Chemistry & Engineering* 7.16 (2019): 14031-14040.
6. Kumar, Viresh, et al. "Enhancement of electrochemical properties of carbon solution doped bismuth ferrite for supercapacitor application." *Materials Today: Proceedings* 41 (2021): 165-171.
7. Sun, Jiale, et al. "Porous CuCo2O4 microtubes as a promising battery-type electrode material for high-performance hybrid supercapacitors." *Journal of Materiomics* 7.6 (2021): 1358-1368.
8. Anjana, R., et al. "Investigations on supercapacitor performance of novel ZnO-CeO2-rGO nanohybrid prepared via hydrothermal method for energy storage applications and their charge storage mechanism." *Diamond and Related Materials* 146 (2024): 111241.
9. Xiong, Pan, et al. "Ternary manganese ferrite/graphene/polyaniline nanostructure with enhanced electrochemical capacitance performance." *Journal of Power Sources* 266 (2014): 384-392.
10. Gnanakumari, DV Ezhilarasi, et al. "Role of ionic nature of surfactants on zinc stannate nanostructure and their application towards supercapacitors." *Discover Electrochemistry* 1.1 (2024): 9.
11. Morad, M. M., R. M. AbouShahba, and M. M. Rashad. "Enhancing the electrochemical performance of spinel zinc stannate by mixing with natural activated carbon as energy-storage material." *Middle East J Appl Sci* 10 (2020): 479.
12. Tan, Bing, et al. "Zinc stannate (Zn2SnO4) dye-sensitized solar cells." *Journal of the American Chemical Society* 129.14 (2007): 4162-4163.
13. Wang, Yanyan, et al. "Synthesis of 3D-nanonet hollow structured Co3O4 for high capacity supercapacitor." *ACS applied materials & interfaces* 6.9 (2014): 6739-6747.
14. Hwang, Daesub, et al. "Hierarchically structured Zn2SnO4 nanobeads for high-efficiency dye-sensitized solar cells." *Scientific reports* 4.1 (2014): 7353.
15. Jaculine, M. Mary, C. Justin Raj, and S. Jerome Das. "Hydrothermal synthesis of highly crystalline Zn2SnO4 nanoflowers and their optical properties." *Journal of alloys and compounds* 577 (2013): 131-137.
16. Khan, Muhammad Najam, et al. "Visible light photocatalysis of mixed phase zinc stannate/zinc oxide nanostructures precipitated at room temperature in aqueous media." *Ceramics International* 40.6 (2014): 8743-8752.
17. Jung, Kyungeun, et al. "Highly efficient amorphous Zn2SnO4 electron-selective layers yielding over 20% efficiency in FAMAPbI3-based planar solar cells." *ACS Energy Letters* 3.10 (2018): 2410-2417.
18. Mali, Sawanta S., Chang Su Shim, and Chang Kook Hong. "Highly porous Zinc Stannate (Zn2SnO4) nanofibers scaffold photoelectrodes for efficient methyl ammonium halide perovskite solar cells." *Scientific Reports* 5.1 (2015): 1-14.
19. Oh, Lee Seul, et al. "Zn2SnO4-based photoelectrodes for organolead halide perovskite solar cells." *The Journal of Physical Chemistry C* 118.40 (2014): 22991-22994.
20. Rovisco, Ana, et al. "Microwave-Assisted Hydrothermal Synthesis of Zn2SnO4 Nanostructures for Photocatalytic Dye Degradation." *Materials Proceedings* 4.1 (2021): 92.
21. Jiang, Ya-Qi, et al. "Hydrothermal syntheses and gas sensing properties of cubic and quasi-cubic Zn2SnO4." *Materials Chemistry and Physics* 129.1-2 (2011): 53-61.
22. Dinesh, S., et al. "Hydrothermal synthesis of zinc stannate (Zn 2 SnO 4) nanoparticles and its application towards photocatalytic and antibacterial activity." *Journal of Materials Science: Materials in Electronics* 27 (2016): 9668-9675.
23. Miyauchi, Masahiro, et al. "Single crystalline zinc stannate nanoparticles for efficient photo-electrochemical devices." *Chemical communications* 46.9 (2010): 1529-1531.
24. Jeronsia, J. Emima, et al. "Hydrothermal synthesis of zinc stannate nanoparticles for antibacterial applications." *Journal of Taibah University for Science* 10.4 (2016): 601-606.

25. Jiang, Ya-Qi, et al. "Hydrothermal syntheses and gas sensing properties of cubic and quasi-cubic Zn2SnO4." *Materials Chemistry and Physics* 129.1-2 (2011): 53-61.
26. Wang, Bang-Yong, et al. "Facile synthesis of fine Zn2SnO4 nanoparticles/graphene composites with superior lithium storage performance." *Journal of Power Sources* 281 (2015): 341-349.
27. Zuo, Wenhua, et al. "Battery-supercapacitor hybrid devices: recent progress and future prospects." *Advanced science* 4.7 (2017): 1600539.
28. Rasoulifard, M. H., MS Seyed Dorraji, and S. Taherkhani. "Photocatalytic activity of zinc stannate: Preparation and modeling." *Journal of the Taiwan Institute of Chemical Engineers* 58 (2016): 324-332.
29. Ali, Monaam Ben, et al. "Hydrothermal synthesis, phase structure, optical and photocatalytic properties of Zn2SnO4 nanoparticles." *Journal of colloid and interface science* 457 (2015): 360-369.
30. Šepelák, Vladimir, et al. "Nonequilibrium structure of Zn 2 SnO 4 spinel nanoparticles." *Journal of Materials Chemistry* 22.7 (2012): 3117-3126.
31. C Khan, Muhammad Najam, and Joydeep Dutta. "Comparison of photocatalytic activity of zinc stannate particles and zinc stannate/zinc oxide composites for the removal of phenol from water, and a study on the effect of pH on photocatalytic efficiency." *Materials Science in Semiconductor Processing* 36 (2015): 124-133.
32. Zhao, Qinqin, et al. "Polyhedral Zn2SnO4: Synthesis, enhanced gas sensing and photocatalytic performance." *Sensors and Actuators B: Chemical* 229 (2016): 627-634.
33. Sivapunniyam, Aarthy, et al. "High-performance liquefied petroleum gas sensing based on nanostructures of zinc oxide and zinc stannate." *Sensors and Actuators B: Chemical* 157.1 (2011): 232-239.
34. Li, Yudong, et al. "Gas Sensor Based on Zn_2SnO_4/SnO_2 Nanocubes for Rapid N-Propanol Detection." *IEEE Transactions on Instrumentation and Measurement* 71 (2022): 1-8.
35. Moździerz, Maciej, et al. "Understanding the electrochemical reaction mechanism to achieve the excellent performance of the conversion-alloying Zn 2 SnO 4 anode for Li-ion batteries." *Journal of Materials Chemistry A* 11.38 (2023): 20686-20700
36. Ji, Xiaoxu, et al. "Facile Synthesis of Carbon-Coated Zn2SnO4 Nanomaterials as Anode Materials for Lithium-Ion Batteries." *Journal of Nanomaterials* 2014.1 (2014): 169373.
37. Saranya, P. E., A. NirmaleshNaveen, and S. Selladurai. "Novel synthesis of spinel zinc stannate (Zn2SnO4) electrode material for supercapacitor applications." *Journal of Chemical and Pharmaceutical Sciences ISSN* 974 (2015): 2115.
38. Nataraj, Nandini, et al. "Synthesis of hexagonal zinc oxide and rod-shaped zinc stannate as an efficient electrocatalyst for electrochemical detection of calcium channel antagonist." *Journal of Molecular Liquids* 385 (2023): 122390.
39. Saafi, I., et al. "Physical investigations and DFT model calculation on Zn2SnO4-ZnO (ZTO-ZO) alloy thin films for wettability and photocatalysis purposes." *Optik* 187 (2019): 49-64.
40. Alpuche-Aviles, Mario A., and Yiying Wu. "Photoelectrochemical study of the band structure of Zn2SnO4 prepared by the hydrothermal method." *Journal of the American Chemical Society* 131.9 (2009): 3216-3224.
41. Zhu, X. J., et al. "Synthesis and performance of Zn2SnO4 as anode materials for lithium-ion batteries by hydrothermal method." *Journal of Power Sources* 189.1 (2009): 828-831.
42. Sun, Guang, Saisai Zhang, and Yanwei Li. "Solvothermal synthesis of Zn2SnO4 nanocrystals and their photocatalytic properties." *International Journal of Photoenergy* 2014.1 (2014): 580615.
43. Wang, Ziying, et al. "Study on highly selective sensing behavior of ppb-level oxidizing gas sensors based on Zn2SnO4 nanoparticles immobilized on reduced graphene oxide under humidity conditions." *Sensors and Actuators B: Chemical* 285 (2019): 590-600.
44. Hosseini, Masoumeh, et al. "Synthesis and characterization of zinc stannate decorated on graphitic carbon nitride and study its potential for degradation of Eriochrome Black T and erythrosine under simulated sunlight." *Arabian Journal of Chemistry* 17.1 (2024): 105395.

45. Panahi, Atefeh, et al. "Simple sonochemical synthesis, characterization of TmVO4 nanostructure in the presence of Schiff-base ligands and investigation of its potential in the removal of toxic dyes." *Ultrasonics Sonochemistry* 95 (2023): 106362.

46. Bhat, Aadil Ahmad, et al. "Bandgap alteration of Zn2SnO4 nanostructures for optical and photo-luminescent applications." *Materials Chemistry and Physics* 306 (2023): 127993

47. Dai, Chao-Shuan, et al. "Hierarchically structured Ni3S2/carbon nanotube composites as high performance cathode materials for asymmetric supercapacitors." *ACS applied materials & interfaces* 5.22 (2013): 12168-12174

48. Young, David L., et al. "Growth and characterization of radio frequency magnetron sputter-deposited zinc stannate, Zn 2 SnO 4, thin films." *Journal of applied physics* 92.1 (2002): 310-319.
49. Shi, Liang, and Yumei Dai. "Synthesis and photocatalytic activity of Zn 2 SnO 4 nanotube arrays." *Journal of Materials Chemistry A* 1.41 (2013): 12981-12986.
50. Danwittayakul, Supamas, et al. "Enhancement of photocatalytic degradation of methyl orange by supported zinc oxide nanorods/zinc stannate (ZnO/ZTO) on porous substrates." *Industrial & Engineering Chemistry Research* 52.38 (2013): 13629-13636.
51. Al-Attafi, Kadhim, et al. "Cubic aggregates of Zn2SnO4 nanoparticles and their application in dye-sensitized solar cells." *Nano energy* 57 (2019): 202-213.
52. Zhang, R., et al. "Highly sensitive formaldehyde gas sensors based on Ag doped Zn2SnO4/SnO2 hollow nanospheres." *Materials Letters* 254 (2019): 178-181.

53. Conway, Brian E. *Electrochemical supercapacitors: scientific fundamentals and technological applications*. Springer Science & Business Media, 2013.

54. Qin, Liping, et al. "Zn2SnO4/graphene composites as anode materials for high performance lithium-ion batteries." *Journal of Alloys and Compounds* 692 (2017): 124-130.

55. Nakhanivej, Puritut, et al. "Effect of Zn: Sn Ratio and Calcination Temperature on Phase Transformation of Zn-Sn-O Compound." *Key Engineering Materials* 675 (2016): 539-543.

56. Zheng, Min, et al. "Mesostructured perovskite solar cells based on Zn2SnO4 Single Crystal Mesoporous Layer with efficiency of 18.32%." *Journal of Alloys and Compounds* 823 (2020): 153730.

57. Qin, Liping, et al. "Zn2SnO4/graphene composites as anode materials for high performance lithium-ion batteries." *Journal of Alloys and Compounds* 692 (2017): 124-130.
58. Zheng, Min, et al. "Mesostructured perovskite solar cells based on Zn2SnO4 Single Crystal Mesoporous Layer with efficiency of 18.32%." *Journal of Alloys and Compounds* 823 (2020): 153730